Available online at www.sciencedirect.com
ScienceDirect
Journal of Computational Physics 227 (2008) 3244–3259
JOURNAL OF COMPUTATIONAL PHYSICS
www.elsevier.com/locate/jcp

Isotropic compact interpolation schemes for particle methods ☆

Philippe Chatelain *,[1], Anthony Leonard

Graduate Aeronautical Laboratories, California Institute of Technology, Pasadena, CA 91125, USA

Received 11 April 2007; received in revised form 3 August 2007; accepted 26 November 2007
Available online 8 December 2007

Abstract

In particle methods, an accuracy degradation can occur because of the distortion of the element positions. A solution consists in the periodic re-initialization of the particles onto regular locations, at the nodes of a lattice. This so-called redistribution works by the interpolation of particle quantities. The present work considers the design of redistribution schemes on general lattices and in particular on lattices with a higher level of symmetry than the usual cubic lattice. Such lattices allow schemes which are more compact and more isotropic. We test our schemes in the context of three-dimensional vortex methods.

PACS: 02.60.Ed; 02.70.Ns; 47.11.+j; 47.32.Cc

Keywords: Interpolation; Particle methods; Vortex methods; Face-centered cubic lattice; Smoothed particle hydrodynamics

1. Introduction

In particle methods such as the vortex element method (VEM) or smoothed particle hydrodynamics (SPH), one is confronted with problems of integration and interpolation over the elements. In particular, this translates into accuracy degradation when the interpolating elements get too far apart in any direction (see [1,2,9]).

One can follow several approaches to tackle this problem. One approach consists in progressively introducing new elements in the domain. While elegant, this approach requires a costly algorithm to find the new elements' positions and strengths (see [4]).

The other approach is to build a whole new set of elements from the old ones. This process must take place every few time steps in order to prevent the particle distribution from getting too distorted. This so-called redistribution consists in interpolating the new strengths at the nodes of a new non-distorted lattice.

☆ Work sponsored by the US Department of Energy under contract No. DE-AC03-98EE50506.
* Corresponding author.
E-mail address: pchatela@inf.ethz.ch (P. Chatelain).
[1] Present address: Computational Science and Engineering Laboratory, ETH Zurich, CAB H83.1, Universitätstrasse 6, CH-8092 Zurich, Switzerland.

0021-9991/$ - see front matter © 2007 Elsevier Inc. All rights reserved.
doi:10.1016/j.jcp.2007.11.039

This work considers the properties of redistribution schemes for a generic lattice and the construction of schemes which display high accuracy, isotropy and in some cases, compactness. We open this paper with a brief summary of the vortex element method in Section 2 as it constitutes a prototypical particle method and will be the basis of our numerical tests. We then discuss the properties of redistribution schemes (Section 3) and propose two approaches for the construction of isotropic schemes in Section 4. We consider lattices with a high degree of symmetry and derive a generalization of Monaghan [12] for the construction of high order schemes.

Our results are then applied to the design of schemes for lattices with high degrees of symmetry, such as the hexagonal and the face-centered cubic lattices.

We close this paper with the numerical application of these schemes in the context of vortex element methods. It is shown that they carry several advantages in terms of compactness and isotropy.

2. The vortex element method

We consider three-dimensional incompressible flow and the Navier–Stokes in vorticity form

$$\frac{\mathrm{D}\boldsymbol{\omega}}{\mathrm{D}t} = (\nabla \mathbf{u}) \cdot \boldsymbol{\omega} + \nu \nabla^2 \boldsymbol{\omega}, \tag{1}$$

$$\nabla \cdot \mathbf{u} = 0, \tag{2}$$

where $\mathbf{u}(\mathbf{x}, t)$ is the velocity field, ν is the kinematic viscosity, and $\boldsymbol{\omega} = \nabla \times \mathbf{u}$ is the vorticity.

The vortex element method discretizes the vorticity field with particles which have positions $\mathbf{x}_i(t)$ and strengths $\boldsymbol{\alpha}_i(t) = \int_{V_i} \boldsymbol{\omega} \mathrm{d}\mathbf{x}$. V_i is the particle volume. The field is then recovered through

$$\tilde{\boldsymbol{\omega}}(\mathbf{x}, t) = \sum_{i=1}^{N} \zeta_\epsilon(\mathbf{x} - \mathbf{x}_i(t)) \boldsymbol{\alpha}_i(t), \tag{3}$$

where ζ_ϵ is a smooth, usually radially symmetric, interpolating kernel.

The kernel smoothing radius ϵ determines the finest resolved scales. As a result, if the flow distorts the particle set and the inter-particle spacing grows beyond ϵ, the interpolation of Eq. (3) loses all accuracy and breaks down as some power of ϵ/h, where h is the particle spacing [1,2]. This so-called loss of overlap will affect any smoothed particle method.

A Helmholtz decomposition is used to represent the velocity field

$$\mathbf{u} = \nabla \phi + \nabla \times \boldsymbol{\psi}; \tag{4}$$

and we use the gauge $\nabla \cdot \boldsymbol{\psi} = 0$. The function ϕ is the scalar potential and the corresponding velocity is irrotational but potentially dilatational. This contribution will be kept at zero for the remainder of this paper. The stream-function is $\boldsymbol{\psi}$ which is related to the vorticity by the Poisson equation

$$\nabla^2 \boldsymbol{\psi} = -\boldsymbol{\omega}. \tag{5}$$

This Poisson problem can be solved through several techniques. In the present work, we use a Green's function approach

$$\boldsymbol{\psi}(\mathbf{x}) = \sum G(\mathbf{x} - \mathbf{x}_i) \boldsymbol{\alpha}_i(t). \tag{6}$$

The curl of $\boldsymbol{\psi}$ and its gradient then give us respectively the velocity and velocity gradient fields which are needed for the evolution equations of the particles positions and strengths. This problem is a N^2-complex problem, which can be made tractable with a fast multipole method [5,13,17].

In three dimensions, the particle discretization of the vorticity field $\tilde{\boldsymbol{\omega}}$ is not necessarily divergence-free. This spurious divergence needs to be kept at a low level. We also note that $\boldsymbol{\omega} = \nabla \times \mathbf{u}$ is clearly solenoidal; this quantity was used in the design of relaxation methods [16,10] and allows the definition of a divergence error

$$E_{\mathrm{div}} = \int |\tilde{\boldsymbol{\omega}} - \boldsymbol{\omega}|^2 \mathrm{d}\mathbf{x}. \tag{7}$$

In addition to relaxation, it has been shown [2] that the choice of the evaluation of the stretching term in Eq. (1) can alleviate this problem [2].

3. Particle redistribution properties

A redistribution scheme has two components: a lattice and an interpolation function. The term lattice is preferred to mesh because it remains a mathematical object and can span an unbounded region of $\mathbb{R}^3$. Concretely, the lattice nodes are never stored in an array; they are generated on demand.

The interpolation rule will be characterized in terms of its smoothness, order of accuracy and support (Fig. 1). We will introduce and generalize some results from Cottet and Koumoutsakos [2]. A central result concerns the order of interpolation. Let us define the new particles with positions $\mathbf{x}_p$ and strengths $\boldsymbol{\alpha}_p$ as

$$\boldsymbol{\alpha}_p = \sum_q \tilde{\boldsymbol{\alpha}}_q W\left(\frac{\mathbf{x}_p - \tilde{\mathbf{x}}_q}{h}\right), \tag{8}$$

in terms of the interpolation function W, the regularized particle spacing h, and the old positions $\tilde{\mathbf{x}}_q$ and strengths $\tilde{\boldsymbol{\alpha}}_q$.

If we consider an interpolated quantity $\sum_p \boldsymbol{\alpha}_p \phi(\mathbf{x} - \mathbf{x}_p)$ e.g. vorticity or velocity, the discrepancy we introduce can be written as

$$E(\mathbf{x}) = \sum_p \tilde{\boldsymbol{\alpha}}_p \phi\left(\mathbf{x} - \tilde{\mathbf{x}}_p\right) - \sum_p \boldsymbol{\alpha}_p \phi\left(\mathbf{x} - \mathbf{x}_p\right) = \sum_p \tilde{\boldsymbol{\alpha}}_p \left[\phi\left(\mathbf{x} - \tilde{\mathbf{x}}_p\right) - \sum_q \phi\left(\mathbf{x} - \mathbf{x}_q\right) W\left(\frac{\mathbf{x}_q - \tilde{\mathbf{x}}_p}{h}\right)\right]$$

The error behavior will thus be dictated by the factor inside the square brackets, which we can express as

$$f(\mathbf{x} - \tilde{\mathbf{x}}_p) = \sum_q \left(\phi\left(\mathbf{x} - \tilde{\mathbf{x}}_p\right) - \phi\left(\mathbf{x} - \mathbf{x}_q\right)\right) W\left(\frac{\mathbf{x}_q - \tilde{\mathbf{x}}_p}{h}\right). \tag{9}$$

To obtain the above expression, we have imposed

$$\sum_q W(\mathbf{x} - \mathbf{x}_q) = 1, \tag{10}$$

which is physically equivalent to the conservation of the extensive quantity carried by the particles, e.g. $\boldsymbol{\omega}$ for the VEM, mass, momentum and energy for SPH. In order to bound f, we expand ϕ about $\mathbf{x} - \mathbf{x}_q$,

$$f(\mathbf{x} - \tilde{\mathbf{x}}_p) = \sum_q \sum_{|\boldsymbol{\beta}|=1\cdots\infty} (-1)^{|\boldsymbol{\beta}|} \left(\mathbf{x}_q - \tilde{\mathbf{x}}_p\right)^{\boldsymbol{\beta}} \partial_{\boldsymbol{\beta}} \phi(\mathbf{x} - \mathbf{x}_q) W\left(\frac{\mathbf{x}_q - \tilde{\mathbf{x}}_p}{h}\right), \tag{11}$$

where $\boldsymbol{\beta} = \boldsymbol{\beta}_1 \cdots \boldsymbol{\beta}_n$ are n-tuples with $|\boldsymbol{\beta}| = \boldsymbol{\beta}_1 + \cdots + \boldsymbol{\beta}_n$. It is readily seen from this last expression that the moments of W will characterize the error behavior, i.e., if

$$\sum_q \mathbf{x}_q^{\boldsymbol{\beta}} W\left(\frac{\mathbf{x} - \mathbf{x}_q}{h}\right) = \mathbf{x}^{\boldsymbol{\beta}} \quad \text{for } 0 \leqslant |\boldsymbol{\beta}| \leqslant m - 1, \tag{12}$$

then

$$E \sim \mathrm{O}(h^m). \tag{13}$$

One may refer to Cottet and Koumoutsakos [2] for a full proof.

Our work focuses on the development and study of interpolation functions W on a different family of lattices. For this reason, we introduce a notation that reflects the arrangement of the new points $\mathbf{x}_\mathbf{n} = h\mathbf{Rn}$, in the

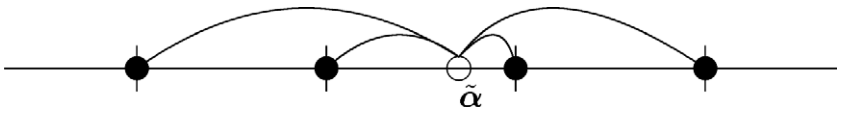

Fig. 1. Redistribution in one dimension: the strength of a particle of the distorted set (open circle) is redistributed onto four nodes (solid circles).

fashion of Merserau [11] and Van De Ville et al. [15]. The columns of the matrix $\mathbf{R}$ are the principal directions of the lattice. Let us also define the matrix $\widehat{\mathbf{R}} = (\mathbf{R}^{-1})^t$ which defines a dual lattice. The lattice step h can be rescaled to unity so it will be dropped from the remainder of this section for the sake of clarity.

Let us now consider the properties of the Fourier transform of the interpolation kernel. The switch to Fourier space will indeed facilitate the development of high order schemes. Theorem 7.2.1 from Cottet and Koumoutsakos [2] and Schoenberg [14] can be generalized to multi-dimensional cases and any kind of lattice as follows.

Theorem 1. *Consider the interpolation formula*

$$Q(\mathbf{x}) = \sum_{\mathbf{n}} q_{\mathbf{Rn}} W(\mathbf{x} - \mathbf{Rn}),$$

where $q_{\mathbf{Rn}}$ is the weight of the point $\mathbf{Rn}$. Let the interpolation function decay fast enough to satisfy the condition

$$|W(\mathbf{x})| \leqslant A\mathrm{e}^{-B|\mathbf{x}|}, \quad \text{where } A > 0,\ B > 0.$$

The formula is of degree m if the following two conditions on $g(k) = \int W(\mathbf{x})\mathrm{e}^{-\mathrm{i}\mathbf{k}\mathbf{x}}\,\mathrm{d}\mathbf{x}$ hold simultaneously:

$$g(\mathbf{k}) - |\mathbf{R}| \text{ has a zero of order } m \text{ at } \mathbf{k} = 0, \tag{14}$$

$$g(\mathbf{k}) \text{ has zeros of order } m \text{ or higher at all } \mathbf{k} = 2\pi\widehat{\mathbf{R}}\mathbf{n} \quad (\mathbf{n} \neq 0). \tag{15}$$

Proof. Let us consider the interpolation function in lattice coordinates $\boldsymbol{\chi}$, $V(\boldsymbol{\chi})$. By definition we have

$$\int V(\boldsymbol{\eta})\,\mathrm{e}^{-\mathrm{i}(\boldsymbol{\kappa}+2\pi\mathbf{n})\cdot\boldsymbol{\eta}}\,\mathrm{d}\boldsymbol{\eta} = \widehat{V}(\boldsymbol{\kappa} + 2\pi\mathbf{n}).$$

Following Cottet and Koumoutsakos [2], we first multiply both sides by $\mathrm{e}^{2\pi\mathrm{i}\mathbf{n}\cdot\boldsymbol{\chi}}$ and sum over $\mathbf{n}$,

$$\sum_{\mathbf{n}} \mathrm{e}^{2\pi\mathrm{i}\,\mathbf{n}\cdot\boldsymbol{\chi}} \int V(\boldsymbol{\eta})\,\mathrm{e}^{-\mathrm{i}(\boldsymbol{\kappa}+2\pi\mathbf{n})\cdot\boldsymbol{\eta}}\,\mathrm{d}\boldsymbol{\eta} = \sum_{\mathbf{n}} \mathrm{e}^{2\pi\mathrm{i}\,\mathbf{n}\cdot\boldsymbol{\chi}}\widehat{V}(\boldsymbol{\kappa} + 2\pi\mathbf{n}). \tag{16}$$

This equation can be simplified thanks to the Poisson summation formula (PSF), which reads

$$\sum_{\mathbf{n}} f(\boldsymbol{\xi} + \mathbf{n}) = \sum_{\mathbf{n}} \mathrm{e}^{2\pi\mathrm{i}\,\mathbf{n}\cdot\boldsymbol{\xi}} \int f(\boldsymbol{\eta})\,\mathrm{e}^{-2\pi\mathrm{i}\,\mathbf{n}\cdot\boldsymbol{\eta}}\,\mathrm{d}\boldsymbol{\eta}. \tag{17}$$

The PSF can be readily applied to the function $f(\boldsymbol{\xi}) = V(\boldsymbol{\xi})\,\mathrm{e}^{-\mathrm{i}\boldsymbol{\kappa}\cdot\boldsymbol{\xi}}$ on the left-hand side of Eq. (16), leaving us with

$$\sum_{\mathbf{n}} \mathrm{e}^{-\mathrm{i}\boldsymbol{\kappa}\cdot(\boldsymbol{\chi}-\mathbf{n})} V(\boldsymbol{\chi} - \mathbf{n}) = \sum_{\mathbf{n}} \mathrm{e}^{2\pi\mathrm{i}\mathbf{n}\cdot\boldsymbol{\chi}}\widehat{V}(\boldsymbol{\kappa} + 2\pi\mathbf{n}). \tag{18}$$

We now reintroduce the physical coordinates $\mathbf{x} = \mathbf{R}\boldsymbol{\chi}$ and define W as $V(\boldsymbol{\chi}) = W(\mathbf{x})$. We have $\widehat{V}(\boldsymbol{\kappa}) = \widehat{W}(\widehat{\mathbf{R}}\boldsymbol{\kappa})/|\mathbf{R}|$ and

$$\begin{aligned}
\sum_{\mathbf{n}} \mathrm{e}^{\mathrm{i}\,\boldsymbol{\kappa}\cdot\mathbf{n}} W(\mathbf{x} - \mathbf{Rn}) &= \mathrm{e}^{\mathrm{i}\boldsymbol{\kappa}\cdot\boldsymbol{\chi}} \sum_{\mathbf{n}} \mathrm{e}^{2\pi\mathrm{i}\,\mathbf{n}\cdot\boldsymbol{\chi}} \frac{\widehat{W}\left(\widehat{\mathbf{R}}\boldsymbol{\kappa} + 2\pi\widehat{\mathbf{R}}\mathbf{n}\right)}{|\mathbf{R}|}, \\
\sum_{\mathbf{n}} \mathrm{e}^{\mathrm{i}\,\mathbf{k}\cdot\mathbf{Rn}} W(\mathbf{x} - \mathbf{Rn}) &= \mathrm{e}^{\mathrm{i}\mathbf{k}\cdot\mathbf{x}} \sum_{\mathbf{n}} \mathrm{e}^{2\pi\mathrm{i}\widehat{\mathbf{R}}\mathbf{n}\cdot\mathbf{x}} \frac{\widehat{W}\left(\mathbf{k} + 2\pi\widehat{\mathbf{R}}\mathbf{n}\right)}{|\mathbf{R}|},
\end{aligned} \tag{19}$$

where we let $\mathbf{k} = \widehat{\mathbf{R}}\boldsymbol{\kappa}$, the physical frequency. We then proceed as in Cottet and Koumoutsakos [2]: we develop $\mathrm{e}^{\mathrm{i}\mathbf{k}\cdot\mathbf{Rn}}$ about 0 in the left-hand side and use the conditions (14) and (15) on the right-hand side

$$\sum_{\nu} \frac{\mathrm{i}^{|\nu|}\mathbf{k}^{\nu}}{\nu!} \sum_{\mathbf{n}} (\mathbf{Rn})^{\nu} W(\mathbf{x} - \mathbf{Rn}) = \mathrm{e}^{\mathrm{i}\mathbf{k}\cdot\mathbf{x}} \frac{\widehat{W}(\mathbf{k})}{|\mathbf{R}|} + \mathcal{O}(\mathbf{k}^m) = \sum_{\nu} \frac{\mathrm{i}^{|\nu|}\mathbf{k}^{\nu}}{\nu!}\mathbf{x}^{\nu} + \mathcal{O}(\mathbf{k}^m).$$

The identification of the coefficients of $\mathbf{k}$ shows that the interpolation is of order m. □

4. Isotropic and compact redistribution schemes

As we have seen above, one can act on either one of the components of a redistribution scheme, the lattice or the interpolation function.

4.1. Hexagonal and face-centered cubic lattices

4.1.1. Properties

The face-centered cubic lattice can be introduced through mathematics or through crystallography, for example. Let us first consider the latter perspective. A lattice can be defined in terms of a unit cell. It is the simplest repeating unit in the crystal, has parallel opposite faces, and its edges connect equivalent points of the lattice.

The face-centered cubic lattice bears its name from the configuration of its unit cell (see Fig. 2). It is cubic and has additional lattice sites at the center of its faces.

The FCC lattice can also be constructed as the periodic stack of two-dimensional hexagonal lattices with the spacing between the layers at $\sqrt{6}/3h$ (Fig. 3(a)). There are three hexagonal lattices in a period A, B and C;

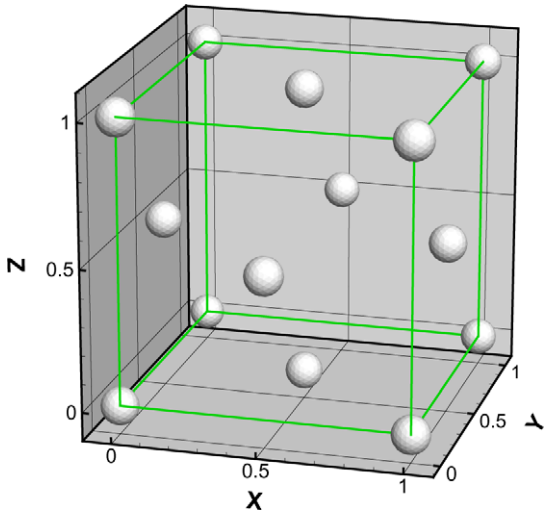

Fig. 2. Face-centered cubic lattice: unit cell.

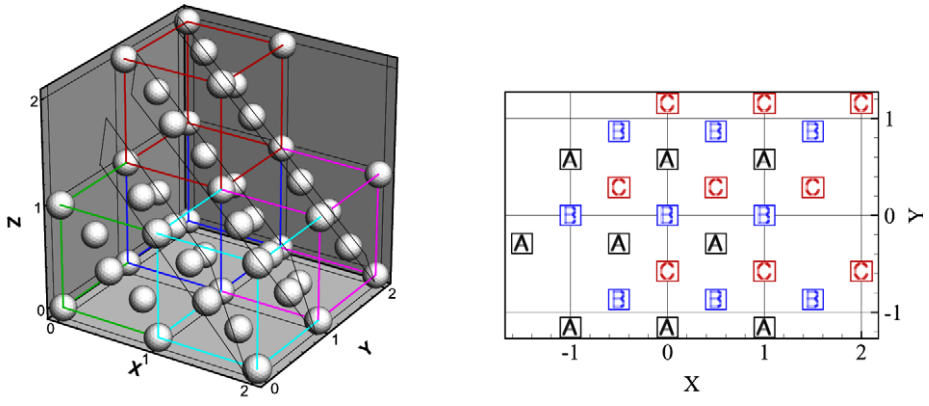

Fig. 3. Face-centered cubic lattice: construction with three families of hexagonal lattices.

if B lies at the origin of the coordinate system in Fig. 3(b), A is shifted by $(-1/2, -\sqrt{3}/6)$ and C, by $(1/2, \sqrt{3}/6)$.

This construction scheme highlights an outstanding feature of this lattice: it corresponds to the packing of spheres. As a matter of fact, the FCC lattice is one of two lattices that pack spheres the most densely. It is also called the Cubic Close Packing lattice. The second lattice to achieve this is the Hexagonal Close Packing lattice which is built from the packing of two families of hexagonal lattices.

On a side note, the question of finding the densest arrangement of spheres is an old and well-known problem in mathematics. Kepler (Strena sue de nive sexangula, 1611) conjectured that the CCP – or FCC – and HCP lattices offered the densest arrangements with a density of $\frac{\pi}{\sqrt{18}} \approx 0.74048$. This conjecture was studied for centuries, starting with Gauss et al. [3] and proved only recently by Hales [6–8].

The equivalent close packing lattice in two dimensions is obviously the hexagonal one which we used in the construction of Fig. 3(b). This lattice already has the interest of the image treatment community [11,15]. On the one hand, it can be the pixel pattern of a sensor that will produce digital images with the same pattern. On the other, it can be interesting to resample and work on digitized images of that nature for their treatment because of the properties of the hexagonal lattice, e.g. edge recognition, etc.

The advantages in our framework are also abundant. A particle method, such as the VEM, may use test and smoothing functions that have spherical–cylindrical in 2D-symmetry. The close packing property is associated with very good symmetry and isotropy; a lattice site is surrounded in 3D by 12 equidistant neighbors, compared to 6 for a cubic lattice. These natural properties can be beneficial in several ways:

(1) The core overlap issue: as mentioned above, the accuracy of interpolation and integration in a particle method decreases when the inter-particle distance becomes larger in any direction than the interpolation kernel radius. This happens in a straining field. One would expect the spatial arrangement of the FCC lattice to help in that respect.
(2) The interaction with boundaries: The FCC lattice can be cut in four planes and still yield a hexagonal lattice with a parameter h. The cubic lattice has only three of these planes. Such a property is of interest in the framework of methods which have to handle boundaries. The boundaries will indeed cut through the lattice in arbitrary directions; the more symmetry, the less noise in quantities measured in the vicinity of the wall or at the wall.
(3) Redistribution functions: The lattice symmetries can be used to design more isotropic and compact schemes.

The matrices $\mathbf{R}$ and $\widehat{\mathbf{R}}$ for the hexagonal and FCC lattices are given in Appendices A and B respectively.

4.1.2. Interpolation functions

Due to the nature of the close packing lattices, we cannot use the tensor product of known one-dimensional functions to interpolate the particles strengths onto the new sites. The use of the lattice coordinates would indeed lead to a non-isotropic redistribution. The scheme construction has to be carried out in two and three

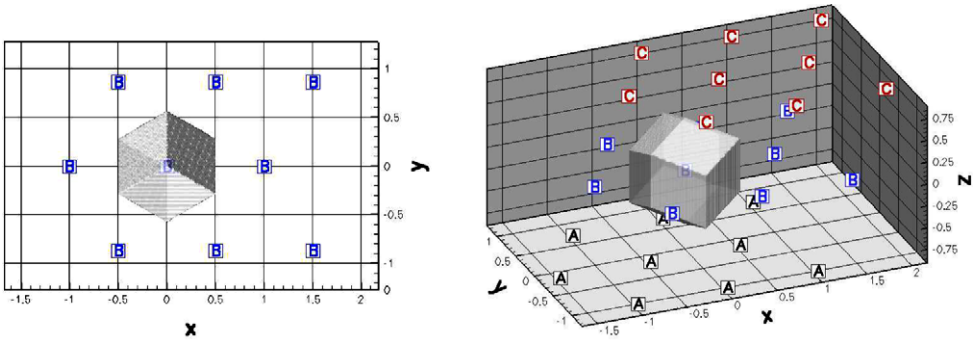

(a) Hexagonal (b) FCC

Fig. 4. The hexagonal and face-centered cubic lattices and their Voronoi cells.

dimensions from the start. We propose two methods to build interpolation functions for the hexagonal and FCC lattices.

4.1.2.1. Splines. In a first approach, one can use the same idea as for one-dimensional splines. It consists in starting from the lowest order "closest-point" function and then taking successive convolutions of this function with itself. For two or three dimensions such a function is also called the indicator function of the *Voronoi* cell $\mathfrak{C}$ [15] and is defined as

$$\chi(\mathbf{x}) = \begin{cases} 1, & \mathbf{x} \in \mathfrak{C}, \\ 1/m_{\mathbf{x}}, & \mathbf{x} \in \partial\mathfrak{C}, \\ 0, & \mathbf{x} \notin \mathfrak{C}, \end{cases} \tag{20}$$

where $m_{\mathbf{x}}$ is number of lattice sites which that position is equidistant to (i.e., in three dimensions, 2 on a face, 3 or more on an edge, etc.). By definition, the tiling of this function over the lattice sites forms a partition of unity (see Fig. 4) and by consequence, the volume of those cells is $\int \chi(\mathbf{x})\mathrm{d}\mathbf{x} = |\mathbf{R}|$. We define the functions $\mathfrak{F}_m$ as

$$\mathfrak{F}_0 = \chi(\mathbf{x}), \tag{21}$$

$$\mathfrak{F}_m = \mathfrak{F}_{m-1} * \mathfrak{F}_0 / \int \mathfrak{F}_0 \,\mathrm{d}x, \tag{22}$$

where we introduced the following notation for the convolution

$$(f * g)(\mathbf{x}) = \int f(\boldsymbol{\xi} - \mathbf{x}) g(\boldsymbol{\xi}) \,\mathrm{d}\boldsymbol{\xi}.$$

One sees that all the $\mathfrak{F}_m$'s will too form a partition of unity. Interestingly enough, the functions for $m \geqslant 1$ show second order accuracy. The Fourier transform of $\mathfrak{F}_0$ is a sine function [15]; it vanishes at the dual lattice sites except the origin, $\widehat{\mathfrak{F}}_0(2\pi\widehat{\mathbf{R}}\mathbf{n}) = |\det(\mathbf{R})|\delta_{\mathbf{n}}$. $\widehat{\mathfrak{F}}_1$ and its successors will therefore present the second order roots at the lattice sites necessary for second order interpolation.

An analytical construction scheme is described in Van De Ville et al. [15] for the hexagonal lattice but it serves a purpose different from ours. The construction therein is used to build increasingly smooth splines with a growing support whereas we are more interested in increasing the order of the redistribution (Eq. (12)) and in keeping the support small, thus preventing the creation of too many new elements.

4.1.2.2. Compact schemes. The nature of the FCC and hexagonal lattices allows the design of simple second order schemes, represented by a piecewise linear function. In 2D, this yields the simple scheme represented in Fig. 5(a). In the three-dimensional case, the interpolation construction is a bit more tedious. To keep the scheme compact and follow the hexagonal lattice example, we need to consider redistribution inside the tetrahedrons and the octahedrons that constitute the face-centered cubic lattice. In a tetrahedron, the function is linear. Inside a octahedron, the function is built piecewise linear to be isotropic, second order, and remain continuous across these different regions.

These schemes (given in Appendices A and B) are arguably the most compact second order schemes. The hexagonal scheme redistributes onto three points. Three degrees of freedom are needed to conserve the first two moments. In three dimensions, the FCC scheme redistributes onto four or six points when four degrees of freedom are needed. With their small support, good conservation properties, and relatively simple analytical expressions, they constitute an interesting starting point to build smoother and higher order interpolations.

As a first step following the method described above for the splines, we take the convolution of these simple schemes by themselves and obtain C^2 schemes (Fig. 5(b)). In doing so, we increase the support of our interpolation.

4.1.2.3. High-order schemes. The second step consists in increasing the order. In the fashion of Monaghan [12], we use the ansatz:

$$\widetilde{W}(\mathbf{x}) = AW + B\mathbf{x} \cdot \nabla W. \tag{23}$$

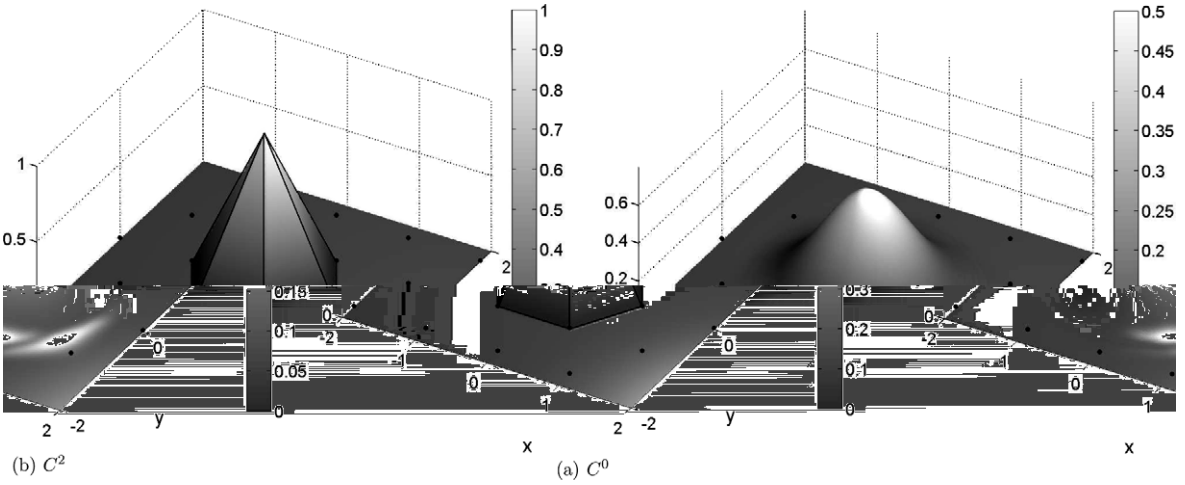

Fig. 5. Second order hexagonal schemes.

The generalization of this result to several dimensions and any type of lattice will be facilitated in Fourier space. Let us assume that the Fourier transform $\widehat{W}$ has, as described in Theorem 1, a zero of order m at the origin and zeros of order $p \geqslant m+2$ at the sites of the dual lattice. An example of such a function is the second order C^2 hexagonal function, for which $m = 2$ and $p = 4$ (Fig. 6). We can use this m-order scheme to build a $(m+1)$-order scheme:

$$\widetilde{W}(\mathbf{x}) = (1 + \frac{n}{m})W + \frac{1}{m}\,\mathbf{x}\cdot\nabla W. \tag{24}$$

Proof. Let us consider the Fourier transform of $\widetilde{W}$,

$$\widehat{\widetilde{W}} = \mathcal{F}(AW + B\mathbf{x}\cdot\nabla W).$$

Using the transform properties of gradients, this becomes

$$\begin{aligned}\widehat{\widetilde{W}} &= A\widehat{W} + B(\mathrm{i}\nabla_{\mathbf{k}})\cdot\mathcal{F}(\nabla W) = A\widehat{W} + B(\mathrm{i}\nabla_{\mathbf{k}})\cdot\left(\mathbf{i}\mathbf{k}\widehat{W}\right) = A\widehat{W} - B(\nabla_{\mathbf{k}}\cdot\mathbf{k})\widehat{W} - B\mathbf{k}\cdot\nabla_{\mathbf{k}}\widehat{W}\\ &= (A - nB)\widehat{W} - B\mathbf{k}\cdot\nabla_{\mathbf{k}}\widehat{W},\end{aligned} \tag{25}$$

where $\nabla_{\mathbf{k}}$ denotes the gradient in Fourier space and $n = \nabla_{\mathbf{k}}\cdot\mathbf{k}$ is the number of dimensions.

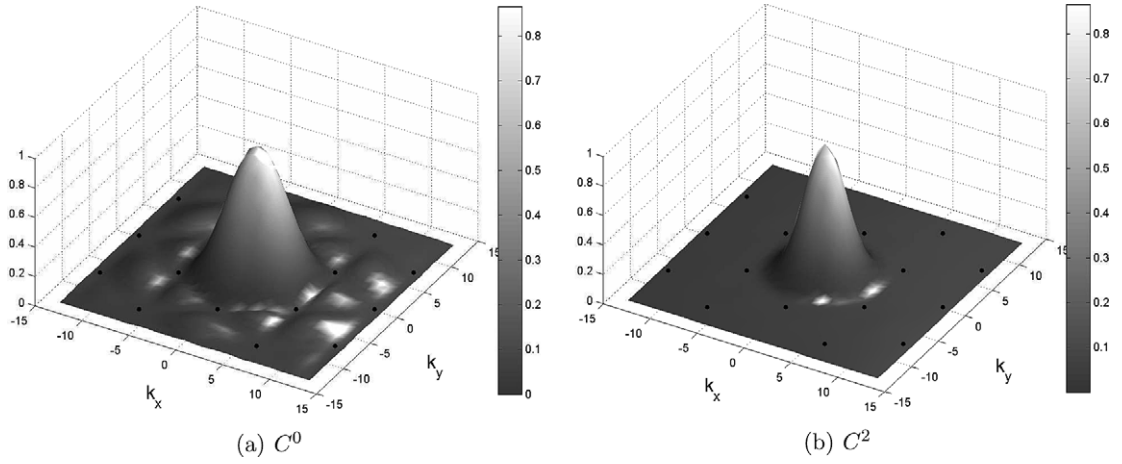

Fig. 6. Fourier transforms of the second order hexagonal schemes.

We will now solve for A and B to meet condition (14). $\widehat{W} - |\mathbf{R}|$ and $\mathbf{k} \cdot \nabla \widehat{W}$ both have a zero of order m at zero. In order to have $\widetilde{W}(0) = |\mathbf{R}|$, we need to impose

$$A - nB = 1. \tag{26}$$

We can increase the order of that root. Developing Eq. (25) about $\mathbf{k} = \mathbf{0}$, we get

$$\begin{aligned}\widehat{\widetilde{W}}(\mathbf{k}) &= |\mathbf{R}| + (-1)^m \frac{\mathbf{M}_{\boldsymbol{\nu}}}{m!}\mathbf{k}^{\boldsymbol{\nu}} - B\mathbf{k}\cdot\nabla\left((-1)^m \frac{\mathbf{M}_{\boldsymbol{\nu}}}{m!}\mathbf{k}^{\boldsymbol{\nu}}\right) + \mathcal{O}\left(\mathbf{k}^{m+1}\right) \\ &= |\mathbf{R}| + (-1)^m \frac{\mathbf{M}_{\boldsymbol{\nu}}}{m!}\mathbf{k}^{\boldsymbol{\nu}} - B(-1)^m \frac{\mathbf{M}_{\boldsymbol{\nu}}}{(m-1)!}\mathbf{k}^{\boldsymbol{\nu}} + \mathcal{O}\left(\mathbf{k}^{m+1}\right),\end{aligned} \tag{27}$$

where $\boldsymbol{\nu}$ is a m-tuple, $1 < \nu_i < n$, $\mathbf{k}^{\boldsymbol{\nu}} = k_{\nu_1} k_{\nu_2} \cdots k_{\nu_p}$, and summation over ν_i is implied. The symmetry of the mth derivatives tensor was also used. If one chooses $B = 1/m$, the extremum at zero will be of order $m + 1$.

Finally, the condition (15) will be satisfied as well because the term, $-B\mathbf{k} \cdot \nabla \widehat{W}$ still has zeros of order $p - 1 \geqslant m + 1$ at all the dual lattice sites $\widehat{\mathbf{R}}\mathbf{n}$. □

Using this result for the second order C^2 functions for the hexagonal and FCC lattices, we obtain the schemes shown in Fig. 7(a) and Fig. 8(a). We see that along with a more compact support (12 and 40 points, respectively), the Hex and FCC schemes show better isotropy than their counterparts on a cubic lattice (Figs. 7(b) and 8(b)) built from the tensor product of 1D schemes.

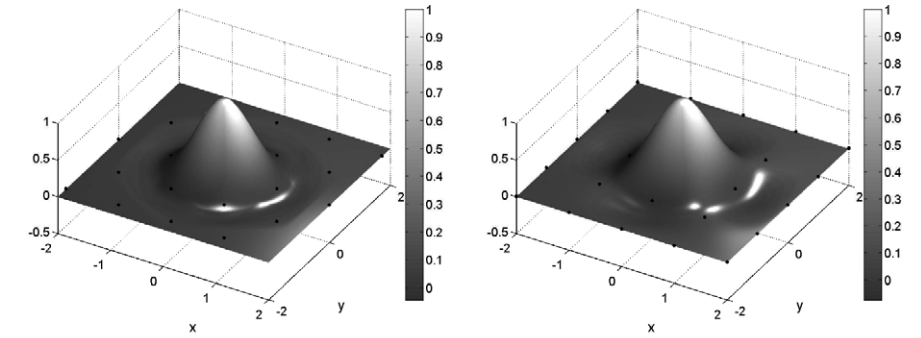

(a) H_3' (b) M_4'

Fig. 7. Third order schemes in the Hexagonal (H_3') and cubic (M_4') lattices.

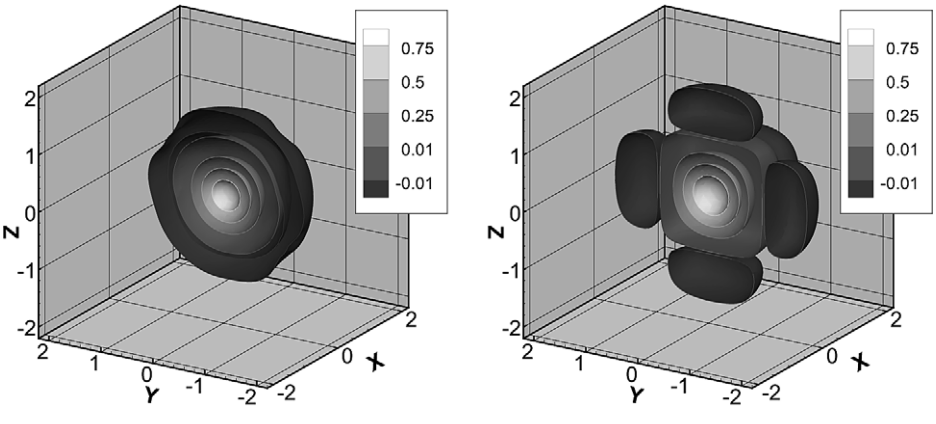

(a) F_3' (b) M_4'

Fig. 8. Third order schemes in the FCC (F_3') and cubic (M_4') lattices.

It is interesting to realize that this order improvement could also be applied to a second order scheme in a cubic lattice. This will obviously yield a scheme different from a tensor product of third order schemes. Let us consider the M'_4 scheme in two dimensions. Built from the tensor product of one-dimensional schemes, it is

$$M'_4(x,y) = \left(\frac{3}{2}M_4(x) + \frac{1}{2}x\frac{\mathrm{d}M_4}{\mathrm{d}x}(x)\right)\left(\frac{3}{2}M_4(y) + \frac{1}{2}y\frac{\mathrm{d}M_4}{\mathrm{d}y}(y)\right).$$

Now applying the above construction in 2D to the scheme $M_4(x,y)$, we get

$$\begin{aligned} M'_{4\,\mathrm{iso}}(x,y) &= 2M_4(x)M_4(y) + \frac{1}{2}(x,y)\cdot\nabla(M_4(x)M_4(y)) \\ &= M'_4(x,y) - (M'_4(x) - M_4(x))(M'_4(y) - M_4(y)). \end{aligned} \tag{28}$$

This scheme has the same order and level of continuity as the regular M'_4, but as shown in Fig. 9, the lobes so characteristic of the tensor product have disappeared. One inconvenience though is the behavior of the scheme at the origin. The scheme does not reach the unit value, $M'_{4\,\mathrm{iso}}(0,0) = \frac{8}{9}$. This is also true to a lesser degree for the third order FCC scheme, F'_3. The value at 0 is 0.95. The third order hexagonal scheme does reach 1.

These two schemes therefore redistribute a particle already at a lattice site onto several sites, creating a slightly weaker particle surrounded by weak particles with positive and negative weights.

5. Application

5.1. Implementation

While the hexagonal functions could all be derived analytically, the high order FCC functions had to be computed. The convolution of the C^0 scheme by itself and the gradient of Eq. (24) were computed in Fourier space. We then switched back to physical space to generate a look-up table.

5.2. Vortex rings reconnections

Our test consists in two vortex rings of equal circulation and geometry in an offset collision (Fig. 10). This configuration initially stretches the rings which align with each other. Reconnections then happen at four

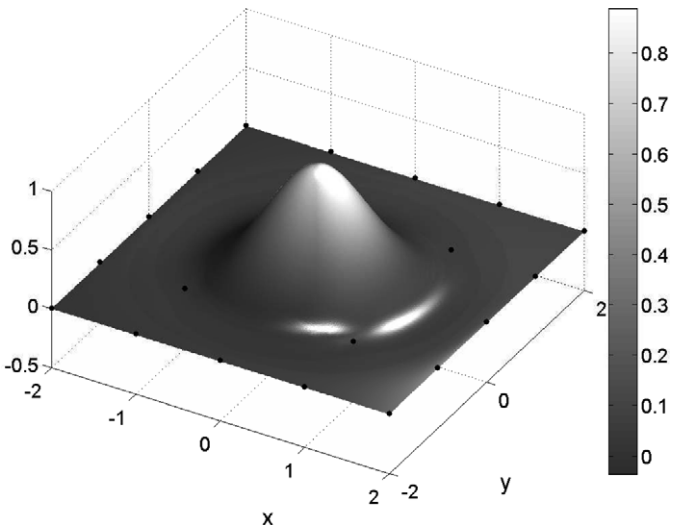

Fig. 9. Isotropic third order scheme in the cubic lattice $M'_{4\,\mathrm{iso}}$.

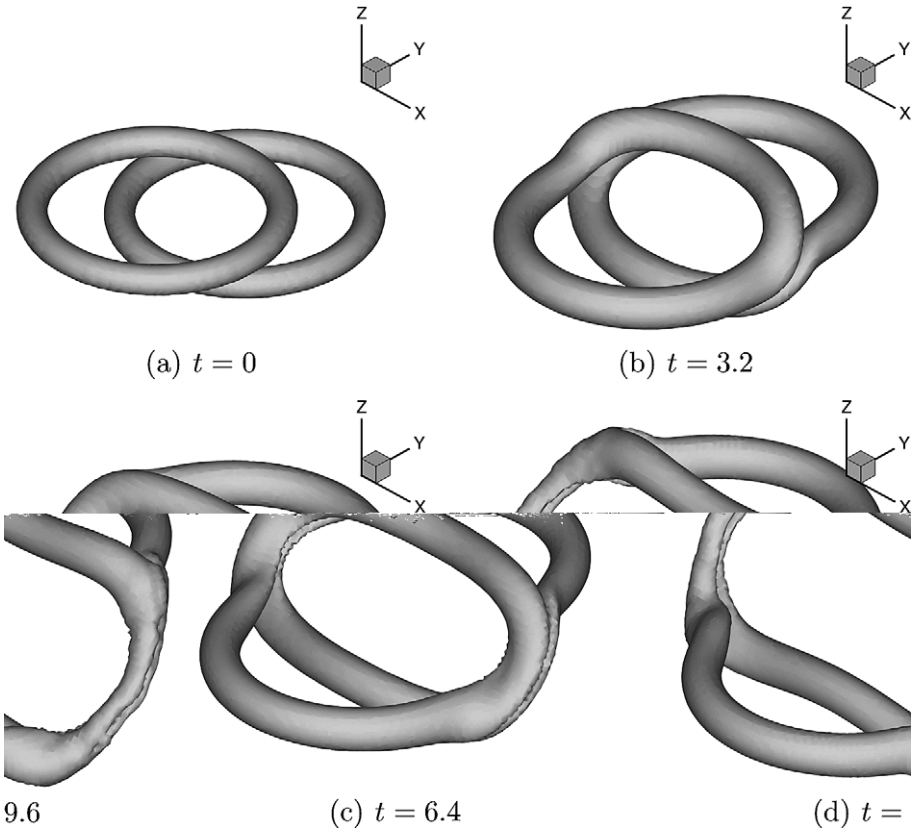

Fig. 10. Collision of two vortex rings with an offset: iso-surface of vorticity $|\omega| = 0.1 \max|\omega(t = 0)|$.

corners (Fig. 10); simultaneously, the secondary structures made of the aligned filaments stretch. This simple configuration subjects the set of particles to deformations; the vorticity vector undergoes re-orientation and stretching in the reconnection regions. The influence of the lattice and of the redistribution can be controlled in several ways. The Courant number based on the velocity gradient and the redistribution frequency indeed determine how much distortion is allowed in our set.

For the remainder of the discussion, our results are made dimensionless in the following manner $t = \frac{\Gamma t'}{R^2}$, $x = \frac{x'}{R}$, $\omega = \frac{R^2\omega'}{\Gamma}$ where t', x', ω' are dimensional. The flow is characterized as follows. The Reynolds number based on the circulation of the rings is $Re_\Gamma = \Gamma/\nu = 1000$. The core radius is 0.1. The initial offset and separation are respectively 0.5 and 0.25.

The numerical parameters were chosen as $\Delta t = 0.32$, $h_{\mathrm{FCC}} = 0.06$ and $h_{\mathrm{CUB}} = 0.054$. We note that $h_{\mathrm{FCC}}|\mathbf{R}_{\mathrm{FCC}}| \simeq h_{\mathrm{CUB}}|\mathbf{R}_{\mathrm{CUB}}|$ to have a similar density of elements in both lattices. The problem is quite under-resolved, the vorticity-based mesh Reynolds number being $Re_h = |\boldsymbol{\omega}|_{\max} h^2/\nu \simeq 40$.

A redistribution is applied every five time steps. A random perturbation is applied to the lattice orientation and its origin to avoid any bias due to the geometry of the problem. The redistribution frequency corresponds to a large strain, which can be evaluated as

$$5\Delta t|\boldsymbol{\omega}|_{\max} \sim 20. \tag{29}$$

We first note that the number of particles grows similarly for both schemes (see Fig. 11). This is an effect of the cutoff used to avoid the creation of weak particles; this cutoff kills more particles in the case of M'_4. For the divergence error, we observe different behaviors. Both schemes start from a nearly identical value of the divergence error. Before any redistribution, the error grows for the cubic lattice and stays stationary for the FCC one. It then jumps at the first redistribution at $t = 1.6$, with a larger jump for the M'_4 scheme. This difference finally decreases as the error creeps up for both schemes.

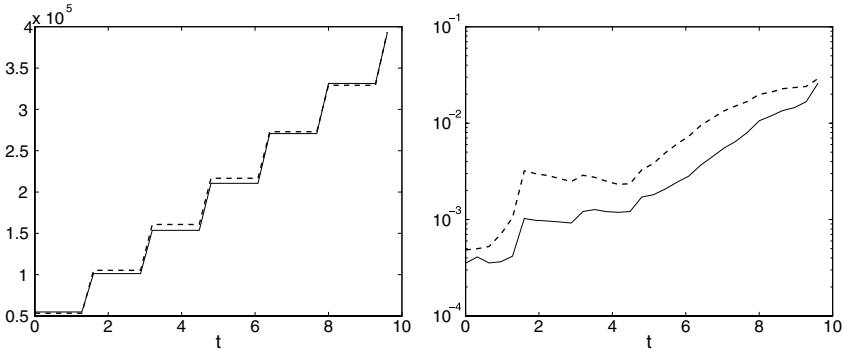

(a) N (b) E_{div}

Fig. 11. Collision of two vortex rings with an offset: number of particles and divergence error, FCC'_3 (solid) and M'_4 (dashed) schemes.

6. Conclusions

We have introduced the first representatives of a new family of interpolation schemes based on the hexagonal and face-centered cubic lattices. Our schemes have two outstanding features:

(1) Thanks to the many symmetries of the underlying lattices, one can design schemes which are more compact than the equivalent ones in a cubic lattice. This results in the creation of fewer particles and a tighter *halo* of new particles around the set of old particles.
(2) Symmetry is also beneficial to the overlap of the particle cores and allows for better communication between the particles, even under stretching. In the context of vortex methods, we have observed a significant reduction in the divergence error in the case of high Re_h.

Appendix A. Hexagonal lattice

The sites of the hexagonal lattice are described as $\mathbf{x_n} = \mathbf{Rn}$, where the matrix $\mathbf{R}$'s columns contain the lattice directions

$$\mathbf{R} = \begin{pmatrix} 1 & 1/2 \\ 0 & \sqrt{3}/2 \end{pmatrix}.$$

There is a dual lattice, defined by the matrix

$$\widehat{\mathbf{R}} = \left(\mathbf{R}^{-1}\right)^t = \begin{pmatrix} 1 & 0 \\ -\sqrt{3}/3 & 2\sqrt{3}/3 \end{pmatrix}.$$

These two lattices and their coordinate systems are presented in Fig. A.1.

A.1. Splines

The family of splines are built from the indicator function of the Voronoi cell

$$\mathfrak{F}_0 = \begin{cases} 1, & \text{if } |\hat{x}| < 0.5 \text{ and } |\hat{y}| < 0.5 \text{ and } |\hat{x} - \hat{y}| < 0.5, \\ 0, & \text{otherwise,} \end{cases} \tag{A.1}$$

where $\hat{x}$ and $\hat{y}$ are dual lattice coordinates. We then take successive convolutions of $\mathfrak{F}_0$ with itself; we get for $\mathfrak{F}_1$

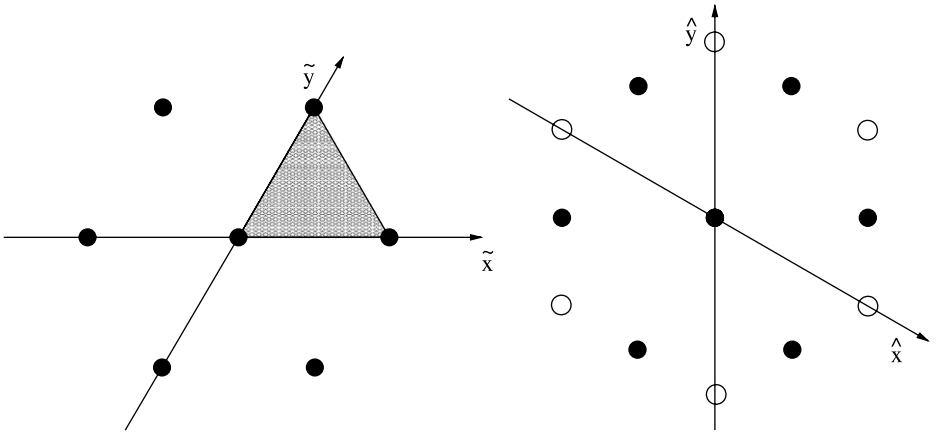

(a) Lattice coordinates (b) Dual lattice coordinates

Fig. A.1. The hexagonal lattice, its dual lattice and their coordinate systems.

$$\mathfrak{F}_1 = \frac{4}{3}\begin{cases} (1-\hat{x}')(1-\hat{x}'-\hat{y}'), & \text{if } |\hat{x}'+\hat{y}'|<1 \text{ and } |\hat{x}'|>0.5, \\ (1-\hat{y}')(1-\hat{x}'-\hat{y}'), & \text{if } |\hat{x}'+\hat{y}'|<1 \text{ and } |\hat{y}'|>0.5, \\ \left((1-\hat{y}')(1-\hat{x}'-\hat{y}')-(0.5-\hat{y}')^2\right), & \text{if } |\hat{x}'|\leqslant 0.5 \text{ and } |\hat{y}'|\leqslant 0.5, \\ 0, & \text{otherwise.} \end{cases} \tag{A.2}$$

For conciseness, we use variables $\hat{x}'$, $\hat{y}'$ that map all the sextant onto the first one

$$\hat{x}' = \begin{cases} |\hat{x}-\hat{y}|, & \text{if } \hat{x}\hat{y}>0 \text{ and } |\hat{x}|>|\hat{y}|, \\ |\hat{x}|, & \text{otherwise,} \end{cases} \tag{A.3}$$

$$\hat{y}' = \begin{cases} |\hat{x}-\hat{y}|, & \text{if } \hat{x}\hat{y}>0 \text{ and } |\hat{x}|<=|\hat{y}|, \\ |\hat{y}|, & \text{otherwise.} \end{cases} \tag{A.4}$$

A.2. Compact schemes

The compact schemes are expressed in the lattice coordinate system. For the C^0 scheme, we have

$$\mathfrak{H}_{C^0} = \begin{cases} 1-\tilde{x}'-\tilde{y}', & \text{if } |\tilde{x}'+\tilde{y}'|<1, \\ 0, & \text{otherwise,} \end{cases} \tag{A.5}$$

where once again we use a mapping to work in the first sextant – the first quarter in the hexagonal lattice coordinate system

$$\tilde{x}' = \begin{cases} |\tilde{x}|, & \text{if } \tilde{x}\tilde{y}>0, \\ |\tilde{x}+\tilde{y}|, & \text{otherwise} \end{cases} \tag{A.6}$$

$$\tilde{y}' = \begin{cases} |\tilde{y}|, & \text{if } \tilde{x}\tilde{y}>0, \\ \min(|\tilde{x}|,|\tilde{y}|), & \text{otherwise.} \end{cases} \tag{A.7}$$

The C^2 scheme is found by convolution of the C^0 scheme by itself

$$\mathfrak{H}_{C^2} = \frac{1}{12}\begin{cases} (\tilde{x}' - \tilde{y}' - 2)(\tilde{x}' + \tilde{y}' - 2)^3, & \text{if } |\tilde{x}' + \tilde{y}'| < 2 \text{ and } \tilde{x}' > 1, \\ (\tilde{y}' - \tilde{x}' - 2)(\tilde{x}' + \tilde{y}' - 2)^3, & \text{if } |\tilde{x}' + \tilde{y}'| < 2 \text{ and } \tilde{y}' > 1, \\ (6 + 12\tilde{x}'\tilde{y}'(\tilde{x}' + \tilde{y}' - 1) & \\ \quad -(\tilde{x}'^2 + \tilde{y}'^2)(12 + 2\tilde{x}'\tilde{y}'), & \text{if } |\tilde{x}' + \tilde{y}'| < 2 \text{ and } \tilde{x}' + \tilde{y}' < 1 \\ \quad +8(\tilde{x}'^3 + \tilde{y}'^3) - \tilde{x}'^4 - \tilde{y}'^4), & \\ (10 - 12(\tilde{x}' + \tilde{y}') + 12\tilde{x}'\tilde{y}' & \\ \quad -2\tilde{x}'\tilde{y}'(\tilde{x}'^2 + \tilde{y}'^2), & \text{if } |\tilde{x}' + \tilde{y}'| < 2 \text{ and } \tilde{x}' + \tilde{y}' \geqslant 1 \\ \quad +4(\tilde{x}'^3 + \tilde{y}'^3) - \tilde{x}'^4 - \tilde{y}'^4), & \\ 0, & \text{otherwise.} \end{cases} \tag{A.8}$$

The third order scheme can then be written as

$$\mathfrak{H}^3_{C^1} = \mathfrak{H}^2_{C^2} + \frac{1}{12}\begin{cases} ((2(\tilde{x}'^2 - \tilde{y}'^2) - 4\tilde{x}' - 2\tilde{y}'), & \text{if } |\tilde{x}' + \tilde{y}'| < 2 \text{ and} \\ (\tilde{x}' + \tilde{y}' - 2)^2), & \tilde{x}' > 1, \\ ((2(\tilde{y}'^2 - \tilde{x}'^2) - 4\tilde{y}' - 2\tilde{x}'), & \text{if } |\tilde{x}' + \tilde{y}'| < 2 \text{ and} \\ (\tilde{x}' + \tilde{y}' - 2)^2), & \tilde{y}' > 1, \\ (-\tilde{x}|\tilde{x}^2(12 - 3\tilde{y} - 2\tilde{x}) + 12\tilde{x}(\tilde{y} - 1) & \\ -\tilde{y}(6 - 6\tilde{y} + \tilde{y}^2)|, & \text{if } |\tilde{x}' + \tilde{y}'| < 1, \\ -\tilde{y}|\tilde{y}^2(12 - 3\tilde{x} - 2\tilde{y}) + 12\tilde{y}(\tilde{x} - 1) & \\ -\tilde{x}(6 - 6\tilde{x} + \tilde{x}^2)|)(-\tilde{x}| - 6 + 6\tilde{x}^2 - 2\tilde{x}^3 & \\ +6\tilde{y} - 3\tilde{x}^2\tilde{y} - \tilde{y}^3|, & \text{if } |\tilde{x}' + \tilde{y}'| < 2 \text{ and} \\ -\tilde{y}| - 6 + 6\tilde{y}^2 - 2\tilde{y}^3, & \tilde{x}' + \tilde{y}' > 1, \\ +6\tilde{x} - 3\tilde{y}^2\tilde{x} - \tilde{x}^3|), & \\ 0, & \text{otherwise.} \end{cases} \tag{A.9}$$

Appendix B. Face-centered cubic lattice

The directions of the FCC lattice and its dual counterpart are given by

$$\mathbf{R} = \begin{pmatrix} 1 & 1/2 & 1/2 \\ 0 & \sqrt{3}/2 & \sqrt{3}/6 \\ 0 & 0 & \sqrt{6}/3 \end{pmatrix}, \quad \widehat{\mathbf{R}} = \begin{pmatrix} 1 & 0 & 0 \\ -\sqrt{3}/3 & 2\sqrt{3}/3 & 0 \\ -\sqrt{6}/6 & -\sqrt{6}/6 & \sqrt{6}/2 \end{pmatrix}. \tag{B.1}$$

B.1. Splines

The first spline is given by

$$\mathfrak{F}_0 = \begin{cases} 1, & \text{if } |\hat{x}| < 0.5 \text{ and } |\hat{y}| < 0.5 \text{ and } |\hat{z}| < 0.5 \\ & \text{and } |\hat{x} - \hat{y}| < 0.5 \text{ and } |\hat{x} - \hat{z}| < 0.5 \text{ and } |\hat{z} - \hat{y}| < 0.5 \\ 0, & \text{otherwise} \end{cases} \tag{B.2}$$

We then get by convolution

$$\mathfrak{F}_1 = \begin{cases} & \text{if } |\hat{x}'| \geqslant 0.5 \text{ and} \\ (1-\hat{x}')(1-\hat{y}')(1-\hat{z}'), & \quad |\hat{y}'| \geqslant 0.5 \text{ and} \\ & \quad |\hat{z}'| \geqslant 0.5, \\ ((1-\hat{x}')(1-\hat{y}')\hat{z}' & \\ \quad +(0.5-A)(B-\hat{y}'+0.5)^2, & \text{if } |\hat{x}'| \geqslant 0.5 \text{ and} \\ \quad +(2/3)(C-\hat{z}')^3, & \quad |\hat{y}'| \geqslant 0.5 \text{ and} \\ \quad +2(0.5-A)(0.5-B)(C-\hat{z}') & \quad |\hat{z}'| < 0.5 \\ \quad +(0.5-B)(A-\hat{x}'+0.5)^2), & \\ ((1-\hat{x}')\hat{y}'\hat{z}' + (1.5-2\hat{x}'+\hat{y}')(0.5-\hat{y}')\hat{z}' & \\ \quad +2(0.5-\hat{x}'+\hat{z}')(0.5-\hat{y}'+\hat{z}')(0.5-\hat{z}'), & \text{if } |\hat{x}'| \geqslant 0.5 \text{ and} \\ \quad +(1-\hat{x}'+\hat{y}')(0.5-\hat{z}')^2 & \\ \quad -2(0.5-\hat{z}'-(\hat{y}'-\hat{z}')/3)(\hat{y}'-\hat{z}')^2) & \\ & \text{if } |\hat{x}'| < 0.5, \\ CD(1-\hat{x}'), & \quad |\hat{y}'| < 0.5 \text{ and} \\ & \quad |\hat{z}'| < 0.5 \text{ and} \\ & \quad (\hat{y}'-\hat{x}') \leqslant -0.5 \\ ((1-\hat{x}')\hat{y}'\hat{z}' & \\ \quad +(1.5-2\hat{x}'+\hat{y}')(0.5-\hat{y}')\hat{z}', & \text{if } |\hat{x}'| \geqslant 0.5 \text{ and} \\ \quad +2(0.5-A)(0.5-B)(C-\hat{z}'), & \quad |\hat{y}'| < 0.5 \text{ and} \\ \quad +(1-\hat{x}'+\hat{y}')(C-\hat{z}')^2, & \quad |\hat{z}'| < 0.5 \text{ and} \\ \quad -2(C-\hat{z}'-B/3)B^2), & \quad (\hat{y}'-\hat{x}') > -0.5, \\ 0, & \text{otherwise}, \end{cases} \tag{B.3}$$

where the variables $\hat{x}'$, $\hat{y}'$, $\hat{z}'$ are the dual lattice variables reordered in decreasing order $\hat{x}' \geqslant \hat{y}' \geqslant \hat{z}'$ and the variables A, B and C are defined as

$$A = \hat{x}' + C - \hat{z}' - 0.5, \tag{B.4}$$

$$B = \hat{x}' + C - \hat{z}' - 0.5, \tag{B.5}$$

$$C = \min(1 + \hat{z}' - \hat{y}', 1 + \hat{z}' - \hat{x}', 0.5), \tag{B.6}$$

$$D = \min(1 + \hat{y}' - \hat{x}', 0.5). \tag{B.7}$$

B.2. Compact schemes

We switch back to the lattice coordinates $\tilde{x}$, $\tilde{y}$, $\tilde{z}$

$$\mathrm{FCC}_1 = \begin{cases} 1 - 0.5(|\tilde{x}'+\tilde{y}'| + |\tilde{y}'+\tilde{x}'| + |\tilde{x}'+\tilde{z}'|), & \text{if } \tilde{x}\tilde{y}\tilde{z}(\tilde{x}+\tilde{y}+\tilde{z}) > 0, \\ \frac{1}{6}(1 + 3(1 - (|\hat{y}'| + |\hat{z}'|)), & \text{if } \tilde{x}\tilde{y}\tilde{z}(\tilde{x}+\tilde{y}+\tilde{z}) < 0 \text{ and} \\ \quad +2|1 - (|\hat{y}'| + |\hat{z}'|)| & \quad \tilde{y}\tilde{z} > 0, \\ \quad -|\hat{x}'+\hat{z}'| - |\hat{x}'+\hat{y}'|), & \\ \frac{1}{6}(1 + 3(1 - (|\hat{z}'| + |\hat{x}'|)) & \text{if } \tilde{x}\tilde{y}\tilde{z}(\tilde{x}+\tilde{y}+\tilde{z}) < 0 \text{ and} \\ \quad +2|1 - (|\hat{z}'| + |\hat{x}'|)| & \quad \tilde{x}\tilde{z} > 0, \\ \quad -|\hat{y}'+\hat{x}'| - |\hat{y}'+\hat{z}'|), & \\ \frac{1}{6}(1 + 3(1 - (|\hat{x}'| + |\hat{y}'|)) & \text{if } \tilde{x}\tilde{y}\tilde{z}(\tilde{x}+\tilde{y}+\tilde{z}) < 0 \text{ and} \\ \quad +2|1 - (|\hat{x}'| + |\hat{y}'|)| & \quad \tilde{x}\tilde{y} > 0, \\ \quad -|\hat{z}'+\hat{y}'| - |\hat{z}'+\hat{x}'|), & \\ 0, & \text{otherwise}. \end{cases} \tag{B.8}$$

FCC_3 was obtained numerically by the convolution of FCC_1 by itself. The high order FCC'_3 was then computed from the combination of FCC_3 with its gradient. These two operations were carried out in Fourier space.

References

[1] J.T. Beale, A. Majda, Vortex methods ii: high order accuracy in two and three dimensions, Math. Comput. 32 (1982) 29–52.
[2] G.-H. Cottet, P. Koumoutsakos, Vortex Methods, Theory and Practice, Cambridge University Press, 2000.
[3] C.F. Gauss, Besprechung des Buchs von L.A. Seeber: Intersuchungen über die Eigenschaften der positiven ternären quadratischen Formen usw, Göttingsche Gelehrte Anzeigen (1831) (reprinted in Werke, 2 (1876), 188–196).
[4] A. Gharakhani, Grid-free simulation of 3rd vorticity diffusion by a high-order vorticity redistribution method, in: 15th AIAA Computational Fluid Dynamics Conference, Anaheim, CA, 2001, AIAA, 2001.
[5] L. Greengard, V. Rokhlin, A fast algorithm for particle simulations, J. Comput. Phys. 73 (1987) 325–348.
[6] T.C. Hales, The sphere packing problem, J. Comput. Appl. Math. 44 (1992) 41–76.
[7] T.C. Hales, Sphere packings i, Discrete Comput. Geometry 17 (1997) 1–51.
[8] T.C. Hales, Sphere packings ii, Discrete Comput. Geometry 18 (1997) 135–149.
[9] P. Koumoutsakos, Multiscale flow simulations using particles, Annu. Rev. Fluid Mech. 37 (2005) 457–487.
[10] A. Leonard, D. Shiels, J. Salmon, G. Winckelmans, P. Ploumhans, Recent advances in high resolution vortex methods for incompressible flows, in: Proceedings 13th AIAA Computational Fluid Dynamics Conference, Snowmass Village, CO, June 29–July 2, 1997, AIAA, 1997, 97-2108.
[11] R.M. Merserau, The processing of hexagonally sampled two-dimensional signals, Proc. IEEE (1979).
[12] J.J. Monaghan, Extrapolating b-splines for interpolation, J. Comput. Phys. 60 (1985) 253–262.
[13] J.K. Salmon, M.S. Warren, Skeletons from the treecode closet, J. Comput. Phys. 111 (1994) 136–155.
[14] I.J. Schoenberg, Cardinal Spline Interpolation, Society for Industrial and Applied Mathematics, Philadelphia, PA, 1973.
[15] D. Van De Ville, T. Blu, M. Unser, W. Philips, I. Lemahieu, R. Van de Walle, Hex-splines: a novel spline family for hexagonal lattices, IEEE Trans. Image Process. (2004).
[16] G.S. Winckelmans, A. Leonard, Contributions to vortex particle methods for the computation of three-dimensional incompressible unsteady flows, J. Comput. Phys. 109 (2) (1993) 247–273.
[17] G.S. Winckelmans, J.K. Salmon, M.S. Warren, A. Leonard, Application of fast parallel and sequential tree codes to computing three-dimensional flows with the vortex element and boundary element methods, in: Second International Workshop on Vortex Flows and Related Numerical Methods, Montréal, August 1995.